ISSN 1070-3284, Russian Journal of Coordination Chemistry, 2024, Vol. 50, No. 1, pp. 73–84. © Pleiades Publishing, Ltd., 2024.

Lanthanide (Sm, Dy) Complexes with the 9,10-Phenanthrenediimine Redox-Active Ligand: Synthesis and Structures

D. K. Sinitsa[a, *], D. P. Akimkina[a, b], T. S. Sukhikh[a], S. N. Konchenko[a], and N. A. Pushkarevsky[a]

[a] *Nikolaev Institute of Inorganic Chemistry, Siberian Branch, Novosibirsk, Russia*

[b] *Novosibirsk State University, Novosibirsk, Russia*

**e-mail: sinitsa@niic.nsc.ru*

Received May 18, 2023; revised June 22, 2023; accepted July 7, 2023

Abstract—The complex formation of the redox-active ligand bis(*N*,*N*'-2,6-diisopropylphenyl)-9,10-phenanthrenediimine (^{Dipp}PDI) with alkaline metal (Li, K) and lanthanide (Sm, Dy) cations is studied. The reduction of ^{Dipp}PDI with an alkaline metal excess affords the dianionic form of the ligand ($^{Dipp}PDA^{2-}$), which crystallizes with the potassium cation as the coordination polymer $[K_2(^{Dipp}PDA)(Thf)_3]$ (Thf is tetrahydrofuran). The reaction of equimolar amounts of the lithium salt with the dianionic form of the ligand and neutral diimine affords the lithium complex with the radical-anion form ($^{Dipp}PSI^{\bullet -}$) crystallized as $[Li(^{Dipp}PSI)(Thf)_2]$. The samarium(III) complex [SmCp*(^{Dipp}PDA)(Thf)] (**I**) is formed by the reduction of ^{Dipp}PDI with samarocene $[SmCp^*_2(Thf)_2]$ (Cp* is pentamethylcyclopentadienide): both the samarium(II) cation and Cp^{*-} anion are oxidized in the reaction. ^{Dipp}PDI does not react with similar ytterbocene. The dysprosium(III) complexes are synthesized by the ion exchange reactions between $DyI_3(Thf)_{3.5}$ and potassium or lithium salt with the $^{Dipp}PDA^{2-}$ dianion. Similar complexes $[Dy(^{Dipp}PDA)I(Thf)_2]$ (**II**^{Thf}) and $[Dy(^{Dipp}PDA)I(Thf)(Et_2O)]$ (**II**^{Et_2O}) are formed in the reactions with the potassium salt depending on the solvent used: a THF–hexane or a diethyl ether–*n*-hexane mixture, respectively. The coordination of the dysprosium cation by the π system of the conjugated fragment of the NCCN ligand is observed in **II**^{Thf}, whereas in **II**^{Et_2O} this coordination is absent. The reaction with $Li_2(^{Dipp}PDA)$ affords the binary complex salt $[Li(Thf)_3(Et_2O)][DyI_2(^{Dipp}PDA)(Thf)]$ (**III**, crystallization from a THF–Et_2O mixture). The crystallization from THF gives the $[Li(Thf)_4][DyI_2(^{Dipp}PDA)(Thf)]$ salt (**III'**) containing the same anion as **III**. The structures of all new complexes are studied by X-ray diffraction (XRD, CIF files CCDC nos. 2260307–2260313).

Keywords: redox-active ligand, phenanthrenediimine, samarium(III), dysprosium(III), lanthanocene, XRD, steric properties of ligand

DOI: 10.1134/S1070328423601012

INTRODUCTION

Redox-active ligands evoke increased interest in the modern coordination chemistry. These ligands (also named "non-innocent") can reversibly change their charge, which makes it possible to extend possibilities of redox transformations in complexes involving these ligands. Many structural types of redox-active ligands are known [1]. Among them, three families of dioxolene and related ligands well-known due to redox tautomerism in their complexes are distinguished: in the neutral form (L^0) these are *o*-quinones, *o*-iminoquinones, and 1,2-phenylenediimines [2]. As a part of a complex, they can accept up to two electrons passing between the neutral, radical-anion, and dianionic forms (Scheme 1a). For the ligands with the substituents in the dioxolene C_6 cycle having similar properties, the typical redox potentials of these transitions ($L^0/L^{-\bullet}$ and $L^{-\bullet}/L^{2-}$) shift to a more reductive range on going from quinones to diimines.

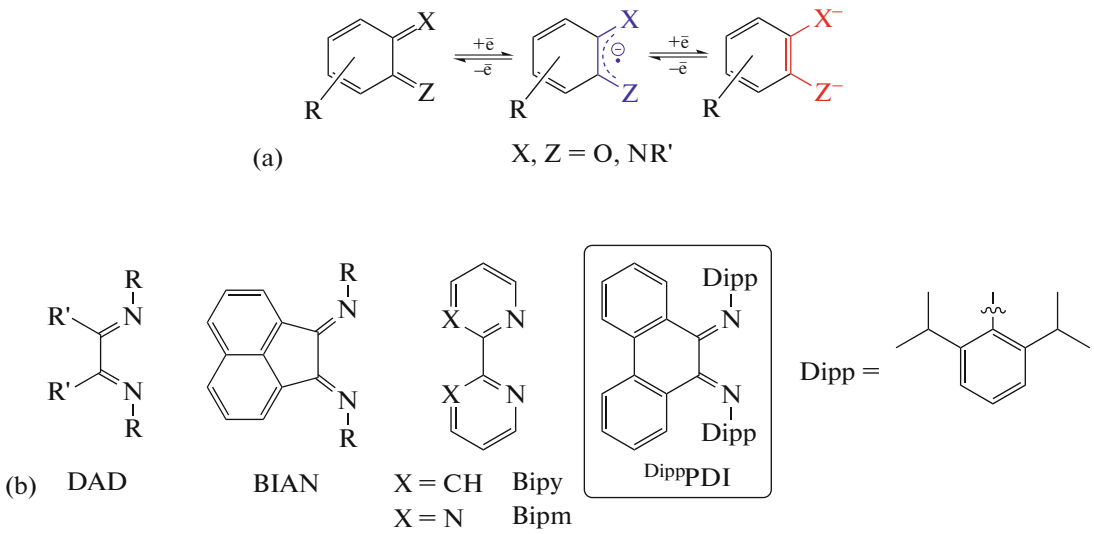

Scheme 1. (a) Generalized structures of the studied ligands and their redox transitions and (b) the most studied types of redox-active diimine ligands and the ligand studied in this work.

Redox transitions in the ligand can be used for the electron transfer in catalytic reactions [3, 4] and the activation or reversible binding of small molecules [5, 6]. A possibility of existing several stable states for complexes with redox-active ligands can be used for the fabrication of units of molecular electronics (for instance, memory elements or switches) and spin labels [7–10]. A combination of these ligands with lanthanide cations (Ln) can result in complexes exhibiting a redox activity unusual for compounds of these metals and demonstrating the magnetic or photophysical properties associated with the redox state of the ligand [11]. The lanthanide complexes with the *o*-quinone ligands are studied rather well [12–14], whereas only single examples are known for the related *o*-iminoquinone [15–18] and *o*-phenylenediimine [19–21] ligands. The redox properties were studied for a series of the neodymium [16], as well as dysprosium and holmium [18] complexes with the redox-active 4,6-di-*tert*-butyl-*N*-(2,6-diisopropylphenyl)-*o*-iminobenzoquinone ligand in different charge states (^{Dipp}IQ, ^{Dipp}ISQ$^{\bullet -}$, ^{Dipp}AP^{2-}), and a possibility of reducing elemental chalcogens due to the dianionic form of the ligand was shown. Higher reduction potentials are needed to reduce substrates with a lower activity, for instance, pnictogens and pnictogenide complexes [22, 23], and they can be achieved using diimine ligands. The lanthanide complexes with related α-diimine (1,4-diaza-1,3-diene (DAD), diiminoacenaphthene (BIAN), and 2,2'-bipyridine/bipyrimidine ligands (Scheme 1b) were studied very well. Different variants of the synthesis were described for them, examples of sterically induced redox transitions are known [24], and a possibility of redox isomerism was shown [25–27]. At the same time, the chemistry of lanthanide complexes with 1,2-phenylenediimine ligands is almost not developed. Only the synthesis and spectroscopic characterization of the series of the Ln complexes with unsubstituted 1,2-phenylenediamine were described [19–21]. However, no data were obtained on the molecular structures of these complexes, and complexes with anionic forms of this ligand are unknown. We have chosen the bis(*N*-2,6-diisopropylphenyl)-9,10-phenanthrenediimine ligand (^{Dipp}PDI) with bulky substituents at the donor nitrogen atoms favoring the formation of molecular complexes. This ligand forms the radical-anion phenanthrenesemidiimine (^{Dipp}PSI$^{\bullet -}$) and dianionic phenanthrenediamide (^{Dipp}PDA^{2-}) forms. Its reactivity for coordination to transition metals and reduction by alkaline metals was described in several works, as well as its reduction properties [28]. The purpose of this work is to study of the synthesis of the lanthanide complexes with this ligand and their structural characterization. Samarium and ytterbium were chosen from the lanthanide series as possessing the accessible Ln^{3+}/Ln^{2+} transitions, and Dy was chosen for comparison with the structures of the known complexes bearing the iminoquinone ligand ^{Dipp}AP^{2-}.

EXPERIMENTAL

All procedures on the synthesis, isolation, and purification of the compounds were carried out in an oxygen-free atmosphere (high-purity argon or vacuum) using the Schlenk technique in evacuated sealed ampules in a glove box with an argon atmosphere. Solvents for the reactions were dehydrated, degassed, and distilled in an inert atmosphere over the Na–K alloy.

The initial lanthanocenes [$LnCp^*_2(Thf)_2$] (Ln = Sm, Yb; Cp* is pentamethylcyclopentadienide; Thf is tetrahydrofuran) [29], dysprosium iodide [$DyI_3(Thf)_{3.5}$] [30], and ^{Dipp}PDI [31] were synthesized using known

procedures. All other reagents were commercially available. IR spectra were recorded on a FT-801 spectrometer (SIMEX) in KBr pellets prepared by pressing in an inert atmosphere. Elemental analysis was carried out on a Vario Micro Cube automated analyzer (Elementar) at the Analytical Laboratory of the Nikolaev Institute of Inorganic Chemistry (Siberian Branch, Russian Academy of Sciences). ^{1}H NMR spectra were recorded on a Bruker Avance 500 spectrometer at a frequency of 500.13 MHz. Signals of the solvent (1.72 ppm for THF-d_8) served as the internal standard. Single crystals for X-ray diffraction (XRD) were selected from the substance mass after the purification and crystallization of the product and were grown in sealed ampules containing the target substance and a minor amount of the solvent stored at the cycled temperature (20–45°C at an interval of 2 h).

Synthesis of [K_2(^{Dipp}PDA)(Thf)$_3$]. *Method* 1. A Schlenk vessel was loaded with ^{Dipp}PDI (200 mg, 0.380 mmol) and an excess of potassium metall (200 mg, 5.13 mmol). THF (10 mL) was condensed to the mixture while cooling, and the resulting mixture was stirred at room temperature for 24 h. In 30 min after the beginning of stirring, the color of the solution changed from red to dark blue with the further gradual change to dark red. The obtained solution was separated from unreacted potassium and evaporated to dryness. Hexane (5 mL) was condensed to the dry residue. The storage of this mixture at room temperature resulted in the formation of red crystals of the product along with a minor amount of the second phase (finely crystalline yellow substance). The crystals of [K_2(^{Dipp}PDA)-(Thf)$_3$] suitable for XRD were taken from the mixture.

Method 2. A Schlenk vessel was loaded with ^{Dipp}PDI (100 mg, 0.190 mmol) and KC_8 (51 mg, 0.38 mmol). THF (10 mL) was condensed to the mixture while cooling, and the resulting mixture was stirred at room temperature for 24 h. In 30 min after the beginning of stirring, the color of the supernatant changed from red to dark blue with the further gradual change to dark red. The solution was separated from a carbon precipitate by filtration and concentrated to 2 mL. Hexane (5 mL) was condensed in vacuo above the solution. The mixture was stored at room temperature to give a finely crystalline red-brown product. The solution was decanted, and the product was dried in vacuo. The yield was 95 mg (61%).

For $C_{50}H_{66}KN_2O_3$

Anal. calcd, %	C, 73.1	H, 8.1	N, 3.4
Found, %	C, 66.7	H, 7.2	N, 3.8

IR (ν, cm^{-1}): 3503 m, 3393 m, 2962 s, 2867 m, 1590 m, 1466 s, 1411 m, 1375 m, 1341 m, 1267 w, 1057 w, 884 w, 790 w, 752 m, 723 m. ^{1}H NMR (THF-d_8; δ, ppm): 0.73 d, 0.84 d, 0.97 d, 1.04 d (all 6H, CH(C$\underline{H}_3$)$_2$, ^3J = 6.8 Hz), 1.77 m (CH_2, THF), 3.32 sept, 3.45 sept (all 2H, C$\underline{H}$(CH$_3$)$_2$, ^3J = 6.8 Hz), 3.62 m (CH_2, THF), 6.18 t (1H, C(2)-H or C(3)-H of phenanthrene, J = 7.3 Hz), 6.53 t (1H, C(3)-H or C(2)-H of phenanthrene, J = 7.5 Hz), 6.73–6.83 m (8H, *m*- and *p*-Dipp, C(5)-H and C(8)-H of phenanthrene), 7.60 m (2H, C(6)-H and C(7)-H of phenanthrene), 8.28 d (1H, C(1)-H or C(4)-H of phenanthrene, J = 7.8 Hz), 8.36 d (1H, C(4)-H or C(1)-H of phenanthrene, J = 7.8 Hz).

Synthesis of [Li(^{Dipp}PSI)(Thf)$_2$]. A Schlenk vessel was loaded with ^{Dipp}PDI (100 mg, 0.190 mmol) and an excess of metallic lithium (10 mg, 1.43 mmol). THF (10 mL) was condensed while cooling to the obtained mixture, and the resulting mixture was stirred at room temperature for 24 h. In 30 min after the beginning of stirring, the color of the solution changed from red to dark blue and further changed to dark red. Unreacted lithium was separated by filtration, and ^{Dipp}PDI (100 mg, 0.190 mmol) was added to the solution on stirring. In an hour, the color of the solution changed to dark blue. The solvent was completely removed in vacuo without heating, and hexane (3 mL) was added to the oily residue. The formed precipitate of the product was filtered off and dried. The yield was 109 mg (85%). The crystals suitable for XRD were grown from a THF–hexane (1 : 3) mixture.

For $C_{46}H_{58}LiN_2O_2$

Anal. calcd., %	C, 81.5	H, 8.6	N, 4.1
Found, %	C, 81.7	H, 8.9	N, 4.1

IR (ν, cm^{-1}): 3393 m, 3058 m, 2960 s, 2867 s, 1590 m, 1455 s, 1425 s, 1381 m, 1361 m, 1338 m, 1262 m, 1108 w, 1045 m, 933 w, 753 s, 721 m, 591 w.

Synthesis of [SmCp*(^{Dipp}PDA)(Thf)] (I). A Schlenk vessel was loaded with [$SmCp^*_2$(Thf)$_2$] (200 mg, 0.350 mmol) and ^{Dipp}PDI (186 mg, 0.350 mmol). THF (10 mL) was condensed while cooling to the obtained mixture, and the solution was stirred at room temperature for 24 h. Then, the initial solvent was completely removed in vacuo without heating, and hexane was added to the solid residue. The formed precipitate of the product was filtered off and washed with hexane (3 × 5 mL). The yield of complex **I** was 254 mg (82%). The crystals suitable for XRD were grown from a THF–hexane (1 : 3) mixture.

For complex $C_{52}H_{65}N_2OSm$ (**I**)

Anal. calcd., %	C, 70.6	H, 7.4	N, 3.2
Found, %	C, 71.0	H, 8.0	N, 2.8

IR (ν, cm^{-1}): 3676 w, 3393 m, 2961 s, 2924 s, 2866 s, 1589 m, 1465 s, 1377 m, 1340 m, 1253 w, 1117 w, 1043 w, 865 w, 790 w, 753 m, 723 m, 572 m.

Synthesis of [DyI(^{Dipp}PDA)(Thf)(solv)] (solv = Thf, $\mathbf{II}^{Thf}$; solv = Et_2O, $\mathbf{II}^{Et_2O}$). A Schlenk vessel was loaded with an excess of metallic potassium (33 mg, 0.84 mmol) and ^{Dipp}PDI (200 mg, 0.380 mmol), and THF (10 mL) was condensed while cooling with liquid nitrogen. In 12 h of stirring at room temperature, a dark red solution of the salt was separated from unreacted potassium, and [$DyI_3(Thf)_{3.5}$] (302 mg, 0.380 mmol) was added to this solution with stirring. The reaction mixture was stirred for 24 h. The formed precipitate of KI was separated by centrifugation, and the solution was evaporated to dryness. Then hexane (5 mL) was condensed into the reaction vessel, and the formed precipitate of the product was filtered off and dried. The yield was 273 mg (75%). Yellow crystals of complexes $\mathbf{II}^{Thf}$ and $\mathbf{II}^{Et_2O}$ suitable for XRD were obtained by recrystallization from a THF–*n*-hexane (1 : 3) or a diethyl ether–*n*-hexane (1 : 3) mixture, respectively.

For complex $C_{46}H_{58}DyIN_2O_2$ ($\mathbf{II}^{Thf}$)

Anal. calcd., %	C, 57.5	H, 6.1	N, 2.9
Found, %	C, 57.7	H, 6.2	N, 3.3

IR (ν, cm^{-1}): 3392 m, 3060 w, 2962 s, 2866 s, 1589 m, 1464 s, 1424 s, 1371 s, 1340 s, 1254 s, 1115 w, 1018 m, 926 w, 863 m, 786 m, 753 s, 723 m, 655 w.

Synthesis of [$Li(Thf)_3(Et_2O)$][DyI_2(^{Dipp}PDA)(Thf)] (III). An excess of metallic lithium (10 mg, 1.4 mmol) and ^{Dipp}PDI (200 mg, 0.380 mmol) were placed in a Schlenk vessel, and THF (10 mL) was condensed while cooling with liquid nitrogen. After 12 h of stirring at room temperature, a dark red solution of the salt was separated from unreacted lithium, and [$DyI_3(Thf)_{3.5}$] (302 mg, 0.380 mmol) was added while stirring. The reaction mixture was stirred at 70°C for 24 h. A yellow-orange solution was concentrated in vacuo to 1 mL, and a LiI precipitate was separated by centrifugation. Diethyl ether (3 mL) was layered on the THF solution. Orange-red crystals were formed due to diffusion. The mother liquor was decanted, and the product was dried in vacuo. The yield was 299 mg (60%).

For complex $C_{58}H_{84}DyI_2LiN_2O_5$ (**III**)

Anal. calcd., %	C, 53.1	H, 6.4	N, 2.1
Found, %	C, 53.0	H, 6.2	N, 2.0

IR (ν, cm^{-1}): 3392 m, 3060 w, 2961 s, 2867 s, 1590 m, 1463 s, 1427 s, 1371 s, 1329 s, 1240 m, 1207 m, 1108 w, 1049 s, 887 m, 859 m, 791 m, 751 s, 722 m, 675 w.

The crystals of complex [$Li(Thf)_4$][DyI_2(^{Dipp}PDA)(Thf)] (**III'**) suitable for XRD were prepared by recrystallization from a THF–*n*-hexane (1 : 3) mixture.

XRD of crystals of [Li(^{Dipp}PSI)$(Thf)_2$], **I**, $\mathbf{II}^{Thf}$, $\mathbf{II}^{Et_2O}$, **III**, and **III'** were carried out at 150 K on a Bruker D8 Venture diffractometer (0.5° ω and φ scan modes, three-circle goniometer with fixed χ, PHOTON III SMOS detector, Mo-IμS 3.0 microfocus source, focusing using Montel mirrors, λ = 0.71073 Å, MoK_α) at the Center for Collective Use at the Nikolaev Institute of Inorganic Chemistry (Siberian Branch, Russian Academy of Sciences). XRD for [K_2(^{Dipp}PDA)$(Thf)_3$] was conducted at 123 K on a Rigaku XtaLAB Synergy-R diffractometer (0.5° ω scan mode, four-circle goniometer, HyPix-Arc 150 hybrid detector, rotating anode source, λ = 1.54184 Å, CuK_α). The primary data were processed using the APEX 3 or CrysAlisPro 1.171.41.107a software. The crystal structures were solved using the ShelXT program [32] and refined using the ShelXL program [33] with the Olex2 graphical interface [34]. Atomic shifts for non-hydrogen atoms were refined in the harmonic anisotropic approximation except for some atoms of the disordered fragments. Hydrogen atoms were arranged geometrically and refined by the riding model. The bond lengths and angles in the studied complexes are given in Table 1, and their crystallographic parameters are listed in Table 2.

The structures were deposited with the Cambridge Crystallographic Data Centre (CIF files CCDC nos. 2260307–2260313; ccdc.cam.ac.uk/structures).

RESULTS AND DISCUSSION

Two different procedures were used for the synthesis of the lanthanide complexes with 9,10-*N*-(2,6-diisopropylphenyl)-*o*-phenanthrenediimine (^{Dipp}PDI). In the first procedure, the redox reactions occur between neutral diimine and lanthanocenes [$LnCp^*_2(Thf)_2$] (Ln = Sm, Yb), whereas the second procedure is based on the exchange reactions between dysprosium triiodide $DyI_3(Thf)_{3.5}$ and salt of the ligand with alkali metal. A good reductive ability of lanthanocenes (due to the oxidation of both lanthanide and ligand Cp^{*-}) is used in the first procedure. However, these initial complexes are accessible only for several lanthanides, and the second procedure does not impose these restraints. Two stages are distinctly observed in the reaction of [$SmCp^*_2(Thf)_2$] and ^{Dipp}PDI in THF (Scheme 2): at first (within 1 h) the ligand is reduced to the radical-anion form, upon which, the solution turns violet and then becomes dark red within several hours, which indicates the formation of the dianionic form. The dark red crystals of complex [SmCp*(^{Dipp}PDA)(Thf)] (**I**) were isolated from a THF–hexane (1 : 3, vol/vol) mixture.

Table 1. Characteristics bond lengths (Å) and angles (°) in the studied complexes and comparison with literature data

Bond or angle	^{Dipp}PDI[a]	[Li(^{Dipp}PSI$^{\bullet-}$)(Thf)$_2$]	[K$_2$(^{Dipp}PDA^{2-})(Thf)$_3$]	**I**	**II**^{Et_2O}	**II**^{Thf}	**III**[b]
C–N[c]	1.27	1.33	1.39, 1.40	1.40, 1.41	1.40, 1.42	1.41	1.42, 1.41/1.40, 1.42
C–C[c]	1.50	1.46	1.42	1.39	1.40	1.41	1.40/1.39
M–N		2.04, 2.01	2.78, 2.86 (K(Thf)$_3$); 2.71, 2.86 (K(Dipp))	2.28, 2.32	2.20, 2.19	2.18, 2.19	2.22, 2.24/2.22, 2.24
Ln–I					3.05	3.03	3.01, 2.99/3.03, 3.01
M–O[d]		2.02, 2.09	2.75, 2.76	2.43	2.38 (Thf) 2.40 (Et$_2$O)	2.37, 2.39	2.42/2.42
NMN		81.0	59.0 (K(Thf)$_3$) 59.9 (K(Dipp))	69.7	76.0	78.0	72.4/71.6

[a] Data from [38].
[b] Data for the complexes with cations [Li(Thf)$_3$(Et$_2$O)]$^+$/[Li(Thf)$_4$]$^+$.
[c] Bonds in the NCCN fragment.
[d] Oxygen atom of coordinated THF or diethyl ether.

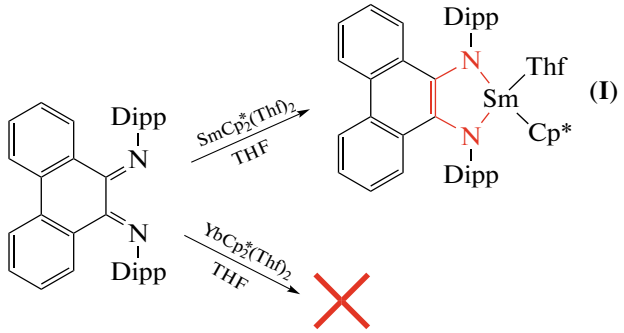

(I)

Scheme 2. Synthesis of the complexes with the ^{Dipp}PDA^{2-} ligand in the redox reactions.

No visible changes are observed in the similar reaction of [YbCp*$_2$(Thf)$_2$] with ^{Dipp}PDI in THF. If the reaction is slow because of blocking the coordination sphere by the donor solvent, then the use of a nonpolar medium could favor its acceleration. However, the reaction does not occur even on prolonged heating the reactants in toluene, and only crystals of the reagents determined visually and from a comparison of the unit cell parameters (XRD) were obtained by crystallization from the solution. We assume two reasons for this behavior. First, ^{Dipp}PDI is rather bulky and, hence, the interaction of the redox-active ligand with the metallocenter can be hindered on decreasing cationic radius and in the presence of other bulky ligands (Cp*$^-$). Second, the reduction potential of the Yb^{3+}/Yb^{2+} pair can be insufficient to reduce the ligand to the radical-anion or dianionic state.

In order the check the last assumption, we studied the electrochemical properties of the ^{Dipp}PDI ligand by cyclic voltammetry (Fig. 1), which revealed the quasi-reversible one-electron reduction at $E_{1/2}$ = −1.85 V (vs. Ag^+/Ag) followed by the irreversible reduction at −2.5 V. Presumably, the first reduction wave corresponds to the transition ^{Dipp}PDI → ^{Dipp}PSI$^{\bullet-}$. Taking into account the redox potential known for lanthanocenes ($E_{1/2}$(LnCp*$_2$(Thf)$_2^{+/0}$) = −2.12 and −1.48 V vs. Ag^+/Ag for Sm and Yb, respectively [35]), we can conclude that the one-electron reduction due to the lanthanide cation is possible in the case of samarium, whereas for ytterbium this process is thermodynamically unfavorable. We failed to isolate the complex with the one-electron reduction product (radical-anion form of the ^{Dipp}PSI$^{\bullet-}$ ligand). This can be associated with the fact that this form is reduced rather rapidly to the dianion. Interestingly, in the reaction with samarocene, the second step of reduction (^{Dipp}PSI$^{\bullet-}$ → ^{Dipp}PDA^{2-}) occurs due to the Cp*$^-$ ligand, which is oxidized and dimerizes to form Cp*$_2$. No reduction due to the Cp*$^-$ ligand occurs in the reaction with ytterbocene. It is most likely, no sufficiently stable complex with the neutral form of the ligand (^{Dipp}PDI) is formed if the reduction step owing to lanthanide is absent, and this form cannot contact rather tightly with the Cp*$^-$ ligand for the electron transfer to occur.

To develop the chemistry of similar complexes with other Ln exhibiting the oxidation state +2, which is less prone to redox processes, alternative synthesis methods are needed, for instance, the ion exchange with lanthanide halides. Therefore, at first it was necessary to prepare anionic forms of the ligand, for example, as salts with alkaline metal cations. Potassium was chosen as a cation due to its lower affinity to form "ate" complexes in the reactions with lanthanide halides. Two synthesis methods were approbated (THF was used as the solvent): the reaction of diimine ^{Dipp}PDI with an excess of metallic potassium or with a stoichiometric amount of potassium-intercalated graphite KC_8 (2 equivalents). In all cases, the color of the solution changed from red to blue and finally to

Table 2. Crystallographic characteristics and experimental and structure refinement details for the compounds studied

Parameter	[Li(^{Dipp}PSI)(Thf)$_2$]	[K$_2$(^{Dipp}PDA)(Thf)$_3$]	**I**	**II**^{Et_2O}	**II**^{Thf}	**III**	**III'**
CCDC no.	2260310	2260308	2260309	2260307	2260313	2260312	2260311
Empirical formula	$C_{46}H_{58}N_2O_2Li$	$C_{50}H_{66}N_2O_3K_2$	$C_{52}H_{65}N_2OSm$	$C_{46}H_{60}N_2O_2IDy$	$C_{46}H_{58}N_2O_2IDy$	$C_{58}H_{84}DyI_2LiN_2O_5$	$C_{58}H_{82}DyI_2LiN_2O_5$
FW	677.88	821.24	884.41	962.36	960.34	1312.51	1310.49
Temperature, K	150(2)	123(2)	150(2)	150(2)	150(2)	150(2)	150(2)
Space group	$P2_1/c$	$Pna2_1$	$P2_1/c$	$P2_1/c$	$P2_1/n$	$P\bar{1}$	$Pna2_1$
a, Å	15.7963(15)	26.2658(3)	16.2847(4)	19.551(3)	11.8045(8)	15.2956(8)	31.493(2)
b, Å	11.8461(11)	13.34900(18)	12.2290(3)	10.0410(16)	36.161(2)	18.7021(11)	14.3689(10)
c, Å	21.1715(16)	12.59996(13)	23.4217(5)	21.681(4)	19.5591(10)	20.4237(12)	12.9322(8)
α, deg	90	90	90	90	90	91.796(2)	90
β, deg	94.582(3)	90	106.4140(10)	93.290(6)	94.094(2)	95.974(2)	90
γ, deg	90	90	90	90	90	90.133(2)	90
V, Å^3	3949.0(6)	4417.82(9)	4474.23(18)	4249.1(12)	8327.7(9)	5807.7(6)	5852.1(7)
Z	4	4	4	4	8	4	4
ρ_{calc}, g/cm^3	1.140	1.235	1.313	1.504	1.532	1.501	1.487
μ, mm^{-1}	0.068	2.227	1.351	2.523	2.574	2.396	2.377
F(000)	1468.0	1768.0	1844.0	1940.0	3864.0	2644.0	2636.0
Crystal size	0.30 × 0.30 × 0.06	0.60 × 0.30 × 0.15	0.16 × 0.12 × 0.10	0.15 × 0.05 × 0.04	0.22 × 0.17 × 0.08	0.22 × 0.17 × 0.08	0.17 × 0.16 × 0.11
Radiation	MoK_α (λ = 0.71073)	CuK_α (λ = 1.54178)	MoK_α (λ = 0.71073)	MoK_α (λ = 0.71073)	MoK_α (λ = 0.71073)	MoK_α (λ = 0.71073)	MoK_α (λ = 0.71073)
Range of data collection over 2θ, deg	4.302–51.36	6.73–146.342	3.792–54.218	4.562–51.542	3.91–55.754	2.914–57.398	4.43–55.818
Ranges of *h, k, l*	$-18 \le h \le 19$, $-14 \le k \le 14$, $-25 \le l \le 25$	$-30 \le h \le 32$, $-16 \le k \le 16$, $-8 \le l \le 15$	$-20 \le h \le 18$, $-15 \le k \le 15$, $-30 \le l \le 24$	$-23 \le h \le 23$, $0 \le k \le 12$, $0 \le l \le 26$	$-15 \le h \le 15$, $-47 \le k \le 47$, $-25 \le l \le 24$	$-20 \le h \le 20$, $-25 \le k \le 25$, $-27 \le l \le 27$	$-41 \le h \le 41$, $-18 \le k \le 18$, $-16 \le l \le 17$
Number of measured reflections	34535	20756	38416	8048	112176	80849	82287
Number of independent reflections (R_{int}, R_σ)	7494 (0.0563, 0.0443)	6932 (0.0227, 0.0246)	9853 (0.0399, 0.0379)	8048 (0.0692, 0.0539)	19653 (0.0743, 0.0545)	29208 (0.0373, 0.0446)	13910 (0.0383, 0.0260)
Number of restraints/ refined parameters	159/559	1/522	0/518	0/480	0/953	138/1274	94/680
GOOF by F^2	1.038	1.034	1.031	1.024	1.061	1.138	1.056
R factor ($I > 2\sigma(I)$)	$R_1 = 0.0672$, $wR_2 = 0.1626$	$R_1 = 0.0455$, $wR_2 = 0.1270$	$R_1 = 0.0305$, $wR_2 = 0.0641$	$R_1 = 0.0434$, $wR_2 = 0.0975$	$R_1 = 0.0517$, $wR_2 = 0.1271$	$R_1 = 0.0780$, $wR_2 = 0.1897$	$R_1 = 0.0274$, $wR_2 = 0.0559$
R factor (all data)	$R_1 = 0.0919$, $wR_2 = 0.1783$	$R_1 = 0.0478$, $wR_2 = 0.1290$	$R_1 = 0.0412$, $wR_2 = 0.0688$	$R_1 = 0.0565$, $wR_2 = 0.1045$	$R_1 = 0.0675$, $wR_2 = 0.1365$	$R_1 = 0.0886$, $wR_2 = 0.1949$	$R_1 = 0.0311$, $wR_2 = 0.0573$
$\Delta\rho_{max}/\Delta\rho_{min}$, e/Å^3	0.79/−0.48	0.76/−0.41	0.83/−0.57	1.94/−1.07	2.62/−1.02	6.29/−2.65	1.25/−1.14
Flack parameter		−0.002(6)					−0.009(3)

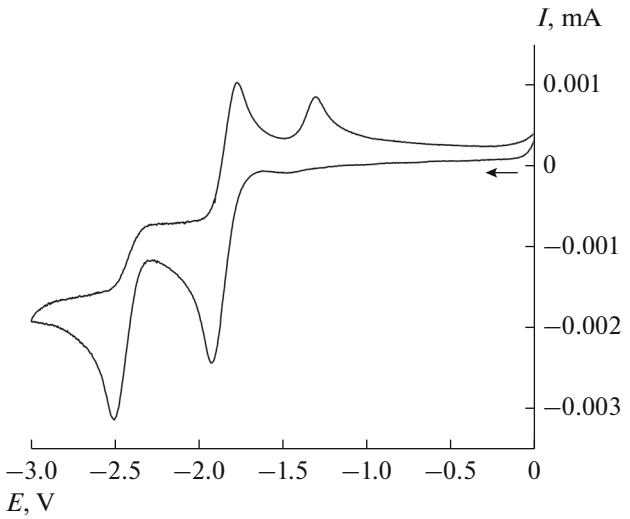

Fig. 1. Cyclic voltammogram of the ^{Dipp}PDI ligand (THF, $V = 0.2$ V/s, vs. Ag^+/Ag, $c = 2 \times 10^{-3}$ mol/L, Pt electrode, Ar, 0.1 M Bu_4NBF_4).

dark red within 3 h. The reaction product is not crystallized when concentrating a THF solution but forms a viscous oil. The finely crystalline product precipitates upon the addition of hexane. Individual crystals of the salt with the dianionic form of the $[K_2(^{Dipp}PDA)(Thf)_3]$ ligand were also prepared by the crystallization from a THF–hexane mixture. Elemental analysis of the polycrystalline sample shows lower values for carbon and hydrogen and higher values for nitrogen. This can be explained by a variable solvate composition of the formed compound, because donor THF molecules are easily leaving and the substance is not resistant to oxidation. The partial loss of THF is confirmed by the ^{1}H NMR spectroscopy data: the integral intensities of signals of the aromatic protons and protons of the *iso*-propyl groups correspond to each other, whereas the intensities of signals from THF are lowered by ~2 times. Therefore, the potassium salt for subsequent syntheses was prepared in situ and used without isolation. When attempting to synthesize the radical-anion form of K(^{Dipp}PSI) by the action of one more equivalent of diimine ^{Dipp}PDI on the in situ prepared dianionic salt, the primarily formed dark blue solution (the color corresponds to the radical anion) rapidly became dark brown. As mentioned [36], the monoanionic forms of diimines, including $^{Dipp}PSI^-$, are unstable but can be stabilized by coordination. The use of the lithium cation made it possible to prepare radical anions stable in solution, which were characterized by EPR. It is most likely that the more ionic character of the K–N bond compared to the more covalent Li–N bond and, as a consequence, the formation of solvate separate ion pairs results in the destabilization of the potassium salt. A similar reaction of a metallic lithium excess with ^{Dipp}PDI followed by the addition of one more equivalent of diimine to the dilithium salt affords a stable dark blue solution from which we succeeded to isolate the pure crystalline phase of the complex with the monoanionic form of the ligand, $[Li(^{Dipp}PSI)(Thf)_2]$.

The salts with alkaline metal cations were used for the synthesis of the dysprosium complexes. A potassium iodide precipitate was formed as a result of the reaction of potassium salt $[K_2(^{Dipp}PDA)(Thf)_3]$ prepared in situ in THF with an equimolar amount of $DyI_3(Thf)_{3.5}$ (Scheme 3). It was difficult to crystallize the product after separating from the precipitate: no crystals were formed by either the slow evaporation of THF, or the replacement of the solvent by toluene. The formed compound was not soluble in hexane. The necessary conditions were achieved for crystallization from a THF–hexane (1 : 3, vol/vol) or a diethyl ether–*n*-hexane (1 : 3, vol/vol) mixture, and molecular complexes $[DyI(^{Dipp}PDA)(Thf)_2]$ (**II**^{Thf}) and $[DyI(^{Dipp}PDA)(Thf)(Et_2O)]$ (**II**^{Et_2O}), respectively, were obtained under these conditions.

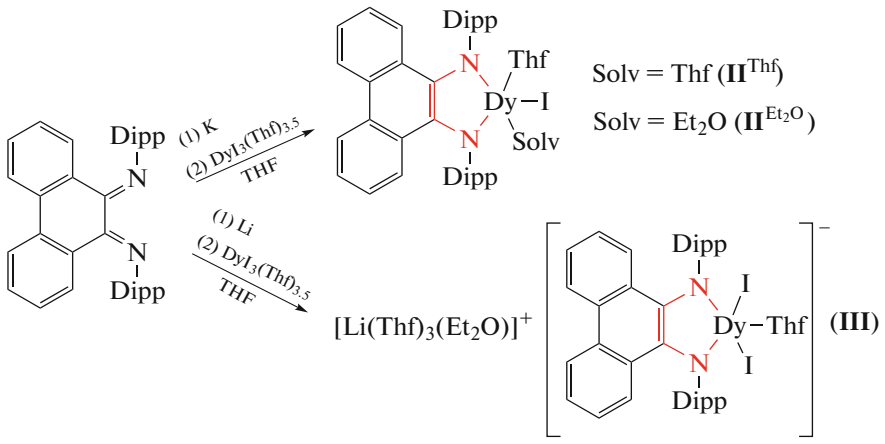

Scheme 3. Synthesis of the complexes by the ion exchange reactions.

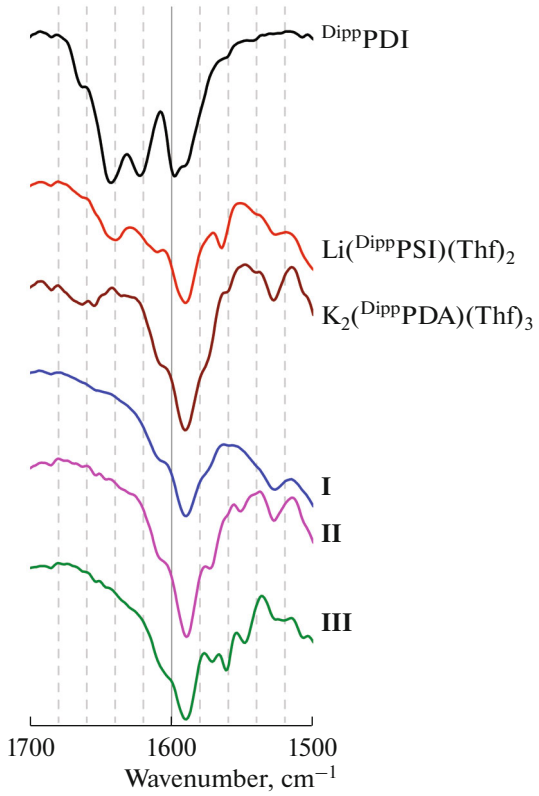

Fig. 2. Characteristic vibrations in the IR spectra of compounds ^{Dipp}PDI, [Li(^{Dipp}PSI)(Thf)$_2$], [K$_2$(^{Dipp}PDA)(Thf)$_3$], **I**, **II**, and **III**.

Interestingly, when the lithium salt prepared in situ by the reduction of neutral diimine ^{Dipp}PDI with an excess of metallic lithium is used in the exchange reaction, the formed complex somewhat differs from the previous complex. The crystallization from a THF–Et_2O (1 : 3, vol/vol) mixture yielded the binary complex salt [Li(Thf)$_3$(Et_2O)][DyI$_2$(^{Dipp}PDA)(Thf)] (**III**). This complex is formed due to a sufficiently high solubility of lithium iodide in THF. Therefore, iodide ions, which enter the composition of the complex as additional anionic ligands, are formed in the solution in a sufficiently high concentration. The crystals of the salt [Li(Thf)$_4$][DyI$_2$(^{Dipp}PDA)(Thf)] (**III'**) with the close composition and containing the same anion as **III** were prepared by crystallization from THF.

The bands in a medium range (1700–1500 cm^{-1}) corresponding to vibrations of the conjugated NCCN system, which depend most strongly on the oxidation state of the ligand, can be distinguished in the IR spectra of ^{Dipp}PDI, [Li(^{Dipp}PSI)(Thf)$_2$], [K$_2$(^{Dipp}PDA)(Thf)$_3$], **I**, **II**, and **III** (Fig. 2). The reduction of ^{Dipp}PDI to ^{Dipp}PSI^{2-} leads to the consecutive decrease in the intensity and the disappearance of the short-wavelength bands at 1620–1650 cm^{-1}, and the long-wavelength band at 1595 cm^{-1} remains nearly unchanged.

The structures of all synthesized complexes were determined by XRD. In [K$_2$(^{Dipp}PDA)(Thf)$_3$], all three THF molecules are coordinated to one of the potassium atoms (Fig. 3a). The second potassium atom is coordinated by the π system of the diisopropylphenyl ring of another molecule of the complex thus joining the complexes into the 1D polymer chain (Fig. 3b). A similar π-coordination was also found in the structures of the alkaline metal salts with the diazabutadiene (DAD) ligand and afforded the tetranuclear complexes [37].

As compared to the potassium salt, the lithium salt with the radical-anion form of the [Li(^{Dipp}PSI)(Thf)$_2$] ligand is the mononuclear complex (Fig. 4). The coordination polyhedron of the compound can be described as a distorted tetrahedron. The C–N and C–C bond lengths in the metallocycles adopt intermediate values between those characteristic of the neutral and dianionic forms (Table 1), which confirms the monoanionic form of the ligand.

In samarium complex **I**, the central atom is coordinated by one η^5-cyclopentadienyl ligand and one phenanthrenediimine ligand (Fig. 5) and the coordination sphere is supplemented by the THF molecule to the coordination number 6. The bond lengths of the NCCN fragment of the metallocycle are close to those in the structure of potassium salt [K$_2$(^{Dipp}PDA)(Thf)$_3$] and correspond to the dianionic form of the ligand ^{Dipp}PDA^{2-} (Table 1). Since the Cp*$^-$ ligand bears a charge of –1, the samarium atom has the oxidation state +3. The bulky ligand Cp*$^-$ is situated in the position opposite to the Sm–N bonds and, thus, the vector Sm–Cp*(centroid) deviates slightly from the SmN$_2$ plane (by 34°). This arrangement is determined by the interaction with the bulky substituents ^{Dipp}PDA^{2-}: the methyl groups of Cp* are arranged closely to the aromatic cycles of both Dipp groups, and a closer arrangement of Cp* is impossible for steric reasons. As a consequence, a less bulky THF ligand occupies the remaining site in the coordination sphere, and the Sm–O bond is directed to the side from the chelate cycle (the angle with the SmN$_2$ plane is 78°).

In the structures of compounds **II**^{Thf} and **II**^{Et_2O}, the coordination polyhedra are nearly the same and represent distorted trigonal bipyramids with the nitrogen and iodine atoms in the equatorial positions and two oxygen atoms in the axial positions (DyIO$_2$N$_2$, coordination number 5; Fig. 6). The diimine ligand exists in the dianionic state, which follows from the composition of the complex and is confirmed by the characteristic values of the C–N and C–C bonds in the chelate cycle (Table 1). The structure of complex **II**^{Thf} contains two independent molecules. The lengths of similar coordination bonds are practically the same for

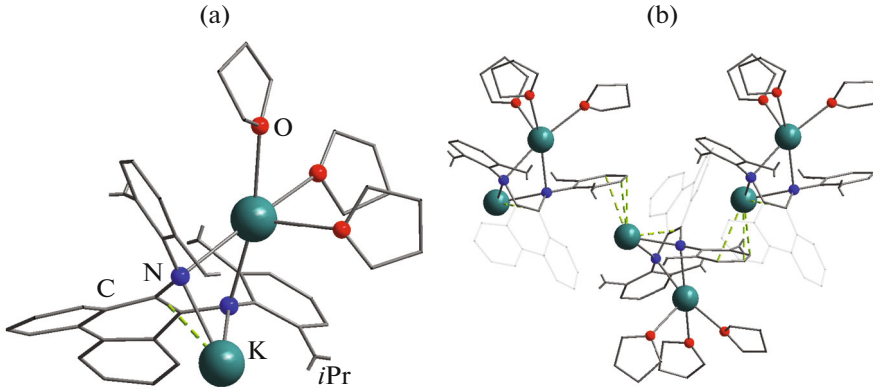

Fig. 3. (a) Structure of the independent part in compound $[K_2(^{Dipp}PDA)(Thf)_3]$ according to the XRD data and (b) the mutual arrangement of three molecules of the complex in the crystal packing. Hydrogen atoms and methyl groups of the Dipp substituents are omitted, hydrocarbon fragments are shown in the simplified form, and π-coordination is shown by dash.

these two molecules, as well as for the complexes $\mathbf{II}^{Thf}$ and $\mathbf{II}^{Et_2O}$. Similarly to complex **I**, the bulky ligand (I^-) is arranged oppositely to the donor nitrogen atoms in the position maximally remote from the Dipp substituents of the diimine ligand. The angle of the Dy–I bond with the DyN_2 plane is 12° and 13° for $\mathbf{II}^{Thf}$ and 0° for $\mathbf{II}^{Et_2O}$. The remaining two accessible coordination sites are occupied by neutral donor THF or Et_2O molecules, and the Dy–O bonds are almost perpendicular to the DyN_2 plane (for all these bonds, the angles with this plane lie in a range of 73°–86°).

Two crystalline phases were obtained for the anionic complex $[Dy(^{Dipp}PDA)I_2(Thf)]^-$: with the $[Li(Thf)_4]^+$ (Fig. 7) and $[Li(Thf)_3(Et_2O)]^+$ cations. The structure with the first cation contains two crystallographically independent cation–anion pairs. The geometry of the anionic complexes is the same in both structures, and the environment of the central atom is DyI_2ON_2 (coordination number 5). As compared to complex **II**, the inclusion of one more large iodide anion into the coordination sphere results in substantial changes in the relative arrangement of the ligands.

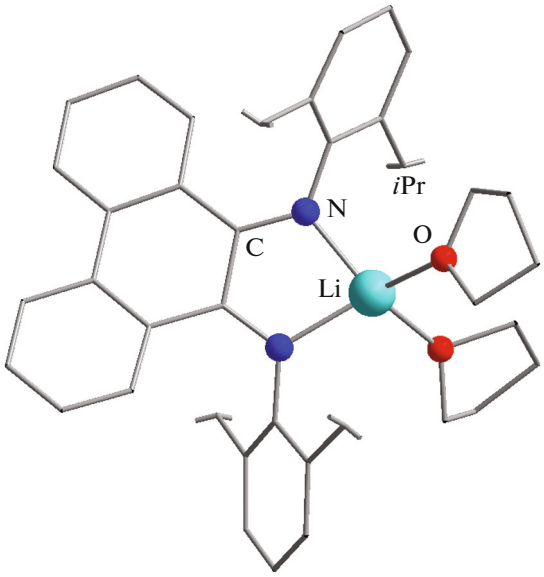

Fig. 4. Structure of $[Li(^{Dipp}PSI)(Thf)_2]$ according to the XRD data. Hydrogen atoms and methyl groups of the Dipp substituents are omitted, and hydrocarbon fragments are shown in the simplified form.

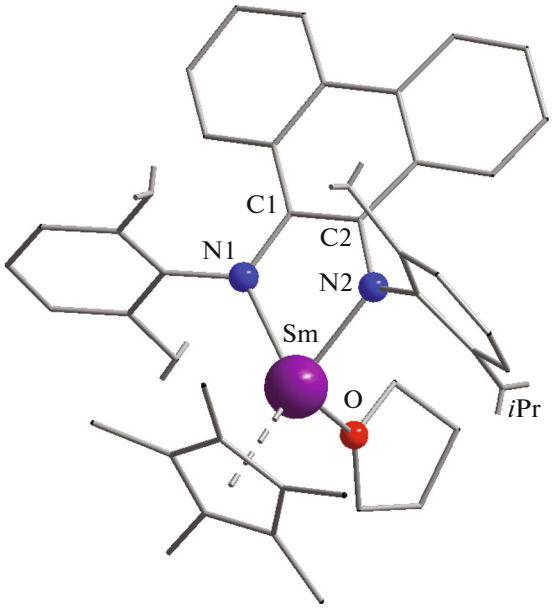

Fig. 5. Structure of complex $[SmCp^*(^{Dipp}PDA)(Thf)]$ (**I**). Hydrogen atoms and methyl groups of the Dipp substituents are omitted, and hydrocarbon fragments are shown in the simplified form.

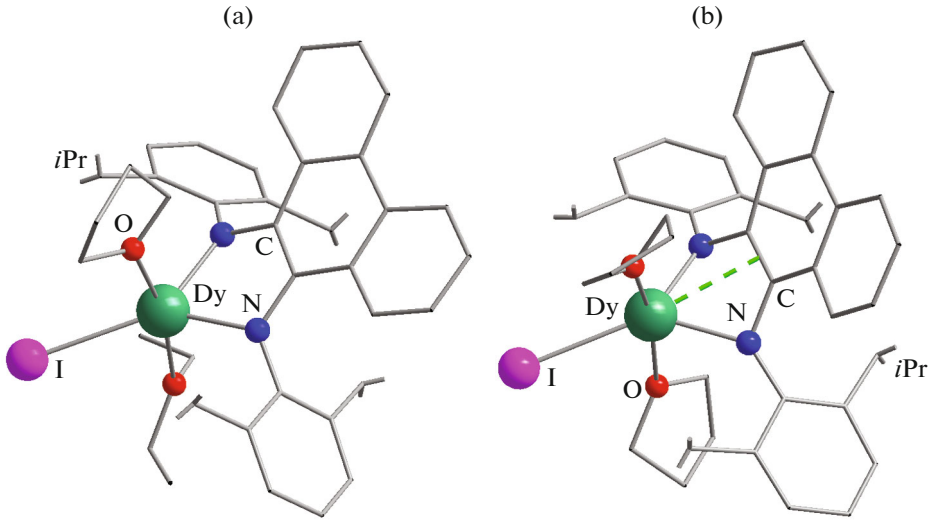

Fig. 6. Structures of complexes (a) [DyI(^{Dipp}PDA)(Thf)(Et_2O)] (**II**^{Et_2O}) and (b) [DyI(^{Dipp}PDA)$(Thf)_2$] (**II**^{Thf}). Hydrogen atoms and methyl groups of the Dipp substituents are omitted, hydrocarbon fragments are shown in the simplified form, and π-coordination is shown by dash.

Two iodide anions cannot be arranged so closely to the diimine ligand as the Et_2O molecules because of the interaction with the bulky Dipp substituents. Therefore, the Dy–I bonds deviate appreciably from the perpendicular to the DyN_2 plane (by 62° and 68°). Both iodine atoms are arranged almost tightly to one of two Dipp substituents, and the remaining site near the second substituent is occupied by one THF molecule. Since the positions at the sides from the DyN_2 plane are occupied by the iodine atoms, the Dy–O bond is situated closely to this plane to form with it an angle of 10°.

It seems interesting to elucidate differences in the position of the metal atom relatively to the chelate cycle in the series of the synthesized complexes. In all structures, the NCCN fragment is nearly planar due to conjugation. The deviation of these four atoms from their root-mean-square plane does not exceed 0.03 Å for the potassium and lanthanide complexes and is maximum in the [Li(^{Dipp}PSI)$(Thf)_2$] complex (0.05 Å). The small lithium cation is localized in the plane of the NCCN fragment (with a distance of 0.05 Å from the plane). In the potassium complex, both cations are remote from this plane at a significant distance (1.65 and 2.39 Å) due to the bridging position of the diimine ligand. In the lanthanide complexes, the metal–nitrogen bond is by ~0.2 Å longer than that in the lithium complex (Table 1). As a consequence, the LnNCCN metallocycle is bent along the line passing through the nitrogen atoms. The samarium atom in complex **I** and dysprosium atoms in complexes **III** and **III'** deviate from the NCCN plane by 0.40–0.47 Å. The dysprosium atoms in complex **II**^{Et_2O} deviate by a slightly higher value (0.74 Å). This can be explained, most likely, by a necessity of arrangement of the bulkier ether ligand (Et_2O) in the gap between the bulky isopropyl groups to minimize the mutual repulsion from them. The structure of compound **II**^{Thf} exhibits the highest deviation of the lanthanide cation from the NCCN plane (1.28 and 1.35 Å) for two independent molecules. Such a substantial deviation results in the situation where the Dy^{3+} cation is located near the C=C double bond of the metallocycle (distance to the bond center 2.66 and 2.64 Å, respectively), which assumes a possibility of the direct coordination of the cation by the π system of the conjugated fragment. The possibility of π-coordination can be assumed to appear in this complex because of the accessible site in the coordination sphere, since the THF molecule occupies a smaller volume than Et_2O (compared to **II**^{Et_2O}). However, it cannot be excluded that the reason is packing effects of the adjacent molecules in the crystal. Anyway, the observed deformation of the coordination cycle demonstrates its considerable flexibility and a possibility of tuning its geometry to various combination of the ligands. A similar structural flexibility has been mentioned previously for the samarium(II) complexes with the N,N-donor β-diketiminate ligands [39].

Thus, the structures of the alkaline metal complexes with the 9,10-phenanthrenediimine ligand in the radical-anion and dianionic states were determined for the first time. The lanthanide complexes with this ligand were demonstrated to be prepared via two routes: via the redox processes involving the neutral form of the ligand and via the exchange reactions with the dianionic form of the ligand. The samarium(III) complex has successfully been synthesized via the first route. However, it was shown that the reduction potential of Yb^{2+} was insufficient for this

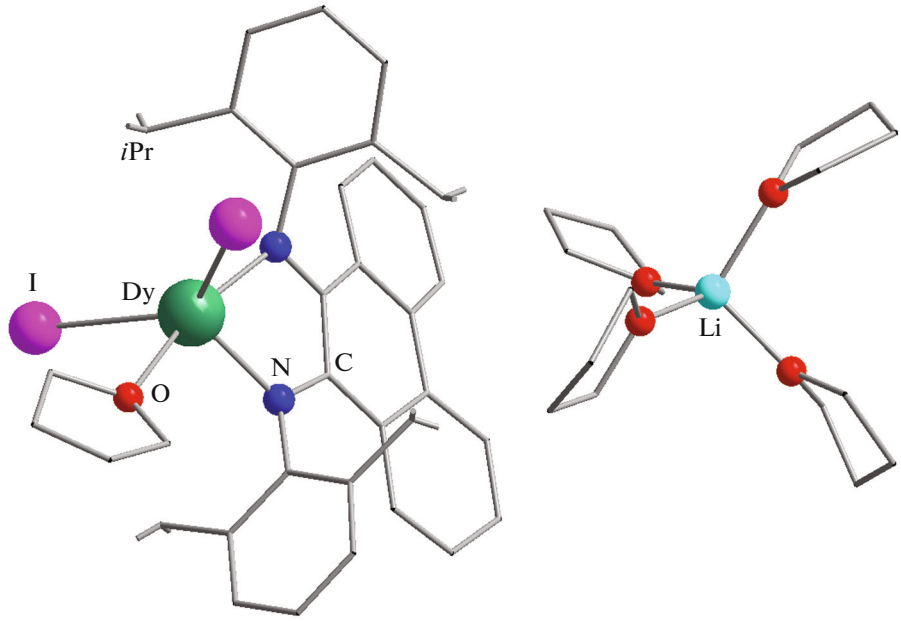

Fig. 7. Structure of the binary complex salt $[Li(Thf)_4][DyI_2(^{Dipp}PDA)(Thf)]$ (**III'**). Hydrogen atoms and methyl groups of the Dipp substituents are omitted, and hydrocarbon fragments are shown in the simplified form.

approach. The dysprosium complexes were synthesized via the second route, and this method can potentially be extended over all lanthanide(III) ions. The structure of the complex synthesized via the ion exchange reactions with LnI_3 was shown to depend on the applied alkaline metal salt. The use of lithium salt results in an increased concentration of the iodide ion and in the anionic complexes bearing two iodide ligands. All lanthanide complexes were formed with the dianionic form of the diimine ligand ($^{Dipp}PDA^{2-}$). Since this form has a sufficiently high reduction potential, the synthesized complexes can manifest the reduction properties due to the oxidation of this form to the radical anion $^{Dipp}PSI^{\bullet -}$, and samarium complex **I** contains also the second ligand potentially capable of being oxidized (Cp^{*-}). The stabilization of the radical-anion form as the lithium complex suggests the stabilization of the lanthanide complexes with this form of the ligand. The reduction properties of the new complexes will be studied in the continuation of this work.

ACKNOWLEDGMENTS

The authors are grateful to the Ministry of Science and Higher Education of the Russian Federation for supporting the work of the Center for Collective Use at the Nikolaev Institute of Inorganic Chemistry (Siberian Branch) and to the workers of the Center for recording ^1H NMR spectra (projects nos. 121031700321-3 and 121031700313-8).

FUNDING

This work was supported by the Russian Science Foundation, project 22-23-00983 (https://rscf.ru/project/22-23-00983/).

CONFLICT OF INTEREST

The authors of this work declare that they have no conflicts of interest.

REFERENCES

1. Kaim, W., *Inorg. Chem.*, 2011, vol. 50, no. 20, p. 9752.
2. Tezgerevska, T., Alley, K.G., and Boskovic, C., *Coord. Chem. Rev.*, 2014, vol. 268, p. 20.
3. Wada, T., Tanaka, K., Muckerman, J.T., and Fujita, E., *Mol. Water Oxid. Catal.*, 2014, p. 77.
4. Kobayashi, K., Ohtsu, H., Wada, T., et al., *J. Am. Chem. Soc.*, 2003, vol. 125, no. 22, p. 6729.
5. Lippert, C.A., Arnstein, S.A., Sherrill, C.D., and Soper, J.D., *J. Am. Chem. Soc.*, 2010, vol. 132, no. 11, p. 3879.
6. Abakumov, G.A., Poddel'sky, A.I., Grunova, E.V., et al., *Angew. Chem., Int. Ed. Engl.*, 2005, vol. 44, no. 18, p. 2767.
7. Bruni, S., Caneschi, A., Cariati, F., et al., *J. Am. Chem. Soc.*, 1994, vol. 116, no. 4, p. 1388.
8. Bubnov, M.P., Kozhanov, K.A., Skorodumova, N.A., et al., *J. Mol. Struct.*, 2019, vol. 1180, p. 878.
9. Piskunov, A.V., Lado, A.V., Fukin, G.K., et al., *Heteroat. Chem.*, 2006, vol. 17, no. 6, p. 481.

10. Kabachnik, M.I., Bubnov, N.N., Solodovnikov, S.P., and Prokof'ev, A.I., *Russ. Chem. Rev.*, 1984, vol. 53, no. 3, p. 288.
11. Hay, M.A. and Boskovic, C., *Chem. A Eur. J.*, 2021, vol. 27, no. 11, p. 3608.
12. Pushkarevsky, N.A., Ogienko, M.A., Smolentsev, A.I., et al., *Dalton Trans.*, 2016, vol. 45, no. 3, p. 1269.
13. Kuzyaev, D.M., Vorozhtsov, D.L., Druzhkov, N.O., et al., *J. Organomet. Chem.*, 2012, vol. 698, p. 35.
14. Caneschi, A., Dei, A., Gatteschi, D., et al., *Dalton Trans.*, 2004, no. 7, p. 1048.
15. Klementyeva, S.V., Lukoyanov, A.N., Afonin, M.Y., et al., *Dalton Trans.*, 2019, vol. 48, no. 10, p. 3338.
16. Coughlin, E.J., Zeller, M., and Bart, S.C., *Angew. Chem., Int. Ed. Engl.*, 2017, vol. 56, no. 40, p. 12142145.
17. Maleev, A.A., Trofimova, O.Y., Pushkarev, A.P., et al., *Nanotechnol. Russ.*, 2015, vol. 10, nos. 7–8, p. 613.
18. Sinitsa, D.K., Sukhikh, T.S., Konchenko, S.N., and Pushkarevsky, N.A., *Polyhedron*, 2021, vol. 195, p. 114967.
19. Subhedar, Y. and Ramachandra, V., *Asian J. Chem.*, 1994, vol. 6, no. 2, p. 277.
20. Ramachandra, V. and Patil, B., *Curr. Sci.*, 1976, vol. 45, no. 19, p. 686.
21. Su, J., He, F., Qi, X., and Wang, J., *Huaxue Yu Shengwu Gongcheng*, 2011, vol. 28, no. 4, p. 36.
22. Schoo, C., Bestgen, S., Egeberg, A., et al., *Angew. Chem., Int. Ed. Engl.*, 2019, vol. 58, no. 13, p. 4386.
23. Reinfandt, N., Michenfelder, N., Schoo, C., et al., *Chem.-Eur. J.*, 2021, vol. 27, no. 29, p. 7862.
24. Trifonov, A.A., Shestakov, B.G., Lyssenko, K.A., et al., *Organometallics*, 2011, vol. 30, no. 18, p. 4882.
25. Fedushkin, I.L., Yambulatov, D.S., Skatova, A.A., et al., *Inorg. Chem.*, 2017, vol. 56, no. 16, p. 9825.
26. Fedushkin, I.L., Maslova, O.V., Baranov, E.V., and Shavyrin, A.S., *Inorg. Chem.*, 2009, vol. 48, no. 6, p. 2355.
27. Fedushkin, I.L., Maslova, O.V., Morozov, A.G., et al., *Angew. Chem., Int. Ed. Engl.*, 2012, vol. 51, no. 42, p. 105847.
28. Groom, C.R., Bruno, I.J., Lightfoot, M.P., and Ward, S.C., *Acta Crystallogr., Sect. B: Struct. Sci., Cryst. Eng. Mater.*, 2016, vol. 72, no. 2, p. 171.
29. Evans, W.J., Grate, J.W., Choi, H.W., et al., *J. Am. Chem. Soc.*, 1985, vol. 107, no. 18, p. 941.
30. Mironova, O.A., Sukhikh, T.S., Konchenko, S.N., and Pushkarevsky, N.A., *Polyhedron*, 2019, vol. 159, p. 337.
31. Cherkasov, V.K., Druzhkov, N.O., Kocherova, T.N., et al., *Tetrahedron*, 2012, vol. 68, no. 5, p. 1422.
32. Sheldrick, G.M., *Acta Crystallogr., Sect. A: Found. Adv.*, 2015, vol. 71, no. 1, p. 3.
33. Sheldrick, G.M., *Acta Crystallogr., Sect C: Struct. Chem.*, 2015, vol. 71, no. 1, p. 3.
34. Dolomanov, O.V., Bourhis, L.J., Gildea, R.J., et al., *J. Appl. Crystallogr.*, 2009, vol. 42, no. 2, p. 339.
35. Veauthier, J.M., Schelter, E.J., Carlson, C.N., et al., *Inorg. Chem.*, 2008, vol. 47, no. 13, p. 5841.
36. Abakumov, G.A., Druzhkov, N.O., Kocherova, T.N., et al., *Dokl. Chem.*, 2016, vol. 467, no. 2, p. 109.
37. Duraisamy, R., Liebing, P., Harmgarth, N., et al., *Eur. J. Inorg. Chem.*, 2019, vol. 2019, no. 28, p. 3343.
38. Gao, B., Luo, X., Gao, W., et al., *Dalton Trans.*, 2012, vol. 41, no. 9, p. 2755.
39. Mironova, O.A., Sukhikh, T.S., Konchenko, S.N., and Pushkarevsky, N.A., *Inorg. Chem.*, 2022, vol. 61, no. 39, p. 15484.

Translated by E. Yablonskaya